Silica Films Having Zigzag Mesoporous Structures with Fixed Kink Angles†

Hirokatsu Miyata,*,‡ Takashi Suzuki,§ Masatoshi Watanabe,‡ Takashi Noma,‡ Kazuhiro Takada,‡ Taihei Mukaide,‡ and Kazuyuki Kuroda*,§,△,⊥

Leading-Edge Technology Development Headquarters, Canon Research Center, Canon Inc., 3-30-2 Shimomaruko, Ohta-ku, Tokyo 146-8501, Japan; Department of Applied Chemistry, Waseda University, 3-4-1 Ohkubo, Shinjuku-ku, Tokyo 169-8555, Japan; Kagami Memorial Laboratory for Materials Science and Technology, Waseda University, 2-8-26 Nishiwaseda, Shinjuku-ku, Tokyo 169-0051 Japan; and CREST, Japan Science and Technology Agency, Japan

Received July 31, 2007. Revised Manuscript Received November 5, 2007

Mesoporous silica films with a highly controlled unique zigzag porous structure are prepared on a rubbing-treated polyimide film. The honeycomb-packed tubular pores in the films have two distinct in-plane alignment directions with respect to the rubbing direction; that is, the films have an in-plane zigzag mesoporous structure with a fixed kink angle. The kink angle is controllable by the molar ratio of tetraethoxysilane as a silica source to surfactant in the reactant solution, and the increase of the ratio results in larger kink angles. The zigzag structure is found to be formed through the formation of an initial immature mesostructured film with uniaxially aligned rodlike surfactant assemblies. It is highly probable that the observed in-plane bending of the pores is caused by the translational shift of the positions of the adsorbed surfactant molecules along the polyimide chains on the surface and that the shift is caused by the steric effects between the adjacent hydrophilic components consisting of surfactant head groups and silica oligomers. The present results show that a unique nanoscale structure, which can hardly be obtained through a reaction under homogeneous conditions, can be formed under the heterogeneous conditions in which the reaction takes place within a restricted environment.

Introduction

The versatility of mesoporous materials, prepared through self-assembly of surfactants,[1–3] comes from the diversity in macroscopic morphology[3–16] as well as those in chemical composition[17–23] and mesoporous structure.[24–26] Among the various morphologies, films[4–8,27–48] are advantageous for

† Part of the "Templated Materials Special Issue".
* To whom correspondence should be addressed.
‡ Canon Inc.
§ Department of Applied Chemistry, Waseda University.
△ Kagami Memorial Laboratory for Materials Science and Technology, Waseda University.
⊥ CREST.

(1) Yanagisawa, T.; Shimizu, T.; Kuroda, K.; Kato, C. *Bull. Chem. Soc. Jpn.* **1990**, *63*, 988.
(2) Kresge, C. T.; Leonowicz, M. E.; Roth, W. J.; Vartuli, J. C.; Beck, J. S. *Nature (London)* **1992**, *359*, 710.
(3) Beck, J. S.; Vartuli, J. C.; Roth, W. J.; Leonowicz, M. E.; Kresge, C. T.; Schmitt, K. D.; Chu, C. T.-W.; Olson, D. H.; Sheppard, E. W.; McCullen, S. B.; Higgins, J. B.; Schlenker, J. L. *J. Am. Chem. Soc.* **1992**, *114*, 10834.
(4) Ogawa, M. *J. Am. Chem. Soc.* **1994**, *116*, 7941.
(5) Lu, Y.; Ganguli, R.; Drewien, C. A.; Anderson, M. T.; Brinker, C. J.; Gong, W.; Guo, Y.; Soyez, H.; Dunn, B.; Huang, M. H.; Zink, J. I. *Nature (London)* **1997**, *389*, 364.
(6) Yang, H.; Kuperman, A.; Coombs, N.; Mamiche-Afara, S.; Ozin, G. A. *Nature (London)* **1996**, *379*, 703.
(7) Aksay, I. A.; Trau, M.; Manne, S.; Honma, I.; Yao, N.; Zhou, L.; Fenter, P.; Eisenberger, P. M.; Gruner, S. M. *Science* **1996**, *273*, 892.
(8) Bruinsma, P. J.; Kim, A. Y.; Liu, J.; Baskaran, S. *Chem. Mater.* **1997**, *9*, 2507.
(9) Huo, Q.; Zhao, D.; Feng, J.; Weston, K.; Buratto, S. K.; Stucky, G. D.; Schacht, S.; Schüth, F. *Adv. Mater.* **1997**, *9*, 974.
(10) Marlow, F.; Spliethoff, B.; Tesche, B.; Zhao, D. *Adv. Mater.* **2000**, *12*, 961.
(11) Miyata, H.; Kuroda, K. *Adv. Mater.* **2001**, *13*, 558.
(12) Grün, M.; Lauer, I.; Unger, K. K. *Adv. Mater.* **1997**, *9*, 254.
(13) Che, S.; Liu, Z.; Ohsuna, T.; Sakamoto, K.; Terasaki, O.; Tatsumi, T. *Nature (London)* **2004**, *429*, 281.
(14) Wu, Y.; Cheng, G.; Katsov, K.; Sides, S. W.; Wang, J.; Tang, J.; Fredrickson, G. H.; Moskovits, M.; Stucky, G. D. *Nat. Mater.* **2004**, *3*, 816.
(15) Schacht, S.; Huo, Q.; Voigt-Martin, I. G.; Stucky, G. D.; Schüth, F. *Science* **1996**, *273*, 768.
(16) Huo, Q.; Margolese, D. I.; Ciesla, U.; Feng, P.; Gier, T. E.; Sieger, P.; Leon, R.; Petroff, P. M.; Schüth, F.; Sucky, G. D. *Nature (London)* **1994**, *368*, 317.
(17) Attard, G. S.; Göltner, C. G.; Corker, J. M.; Henke, S.; Templer, R. H. *Angew. Chem., Int. Ed. Engl.* **1997**, *36*, 1315.
(18) Ying, Y.; Mehnert, C. P.; Wong, M. S. *Angew. Chem., Int. Ed.* **1999**, *38*, 56.
(19) Joo, S. H.; Choi, S. J.; Oh, I.; Kwak, J.; Liu, Z.; Terasaki, O.; Ryoo, R. *Nature (London)* **2001**, *412*, 169.
(20) Inagaki, S.; Guan, S.; Fukushima, Y.; Ohsuna, T.; Terasaki, O. *J. Am. Chem. Soc.* **1999**, *121*, 9611.
(21) Kimura, T.; Sugahara, Y.; Kuroda, K. *Chem. Mater.* **1999**, *11*, 508.
(22) MacLachlan, M. J.; Coombs, N.; Bedard, R. L.; White, S.; Thompson, L. K.; Ozin, G. A. *J. Am. Chem. Soc.* **1999**, *121*, 12005.
(23) Zhao, D.; Feng, J.; Huo, Q.; Melosh, N.; Fredrickson, G. H.; Chmelka, B. F.; Stucky, G. D. *Science* **1998**, *279*, 548.
(24) Zhao, D.; Huo, Q.; Feng, J.; Chmelka, B. F.; Stucky, G. D. *J. Am. Chem. Soc.* **1998**, *120*, 6024.
(25) Tanev, P. T.; Pinnavaia, T. J. *Science* **1995**, *267*, 865.
(26) Huo, Q.; Leon, R.; Petroff, P. M.; Stucky, G. D. *Science* **1995**, *268*, 1324.
(27) Ogawa, M. *Chem. Commun.* **1996**, 1149.
(28) Fan, H.; Lu, Y.; Stump, A.; Reed, S. T.; Baer, T.; Schunk, R.; Perez-Luna, V.; López, G. P.; Brinker, C. J. *Nature (London)* **2000**, *405*, 56.
(29) Doshi, D. A.; Gibaud, A.; Goletto, V.; Lu, M.; Gerung, H.; Ocko, B.; Han, S. M.; Brinker, C. J. *J. Am. Chem. Soc.* **2003**, *125*, 11646.
(30) Miyata, H.; Kuroda, K. *J. Am. Chem. Soc.* **1999**, *121*, 7618.
(31) Miyata, H.; Kuroda, K. *Chem. Mater.* **2000**, *12*, 49.
(32) Miyata, H.; Noma, T.; Watanabe, M.; Kuroda, K. *Chem. Mater.* **2002**, *14*, 766.

10.1021/cm702120m CCC: $40.75
Published on Web 12/11/2007

applications to optical and electronic devices. A wide variety of mesoporous films with various compositions[36–44] and local porous structures[45–48] are formed by optimizing the synthetic conditions and starting chemicals.

Macroscopic-scale control of the porous structure is an important issue for application of mesoporous films. Several methods, such as the use of reactant flow[49–51] and shear stress,[52] have been proposed so far to achieve the alignment of pores in mesoporous silica films. We have demonstrated that the alignment of tubular mesopores can be controlled through the interactions at a solid−liquid interface.[30–33] Both anisotropic atomic arrangements of crystalline substrates[30] and polymeric films with structural anisotropy[31–33] can orient tubular mesopores to a preferred direction. Recently, we demonstrated a strict control of the in-plane arrangement of spherical pores on macroscopic scales and showed the formation of a film with a single crystalline mesoporous structure of $P6_3/mmc$.[34,35]

The mesoporous silica films reported so far, in which the porous structures are macroscopically controlled, have porous structures that are commonly observed in other morphologies such as powders and monolithic forms. However, it is known that mesoporous silicas with unique morphologies can have unusual porous structures. For example, a spiral porous structure is formed in mesoporous silica fibers.[10] It was also reported that mesoporous silica formed in a confined environment, in nanoholes of porous anodic alumina, shows unique porous structures, depending on the structure of the porous host membrane.[14]

Here, we demonstrate the formation of mesoporous silica films with an unprecedented unique porous structure, which has not been observed in the other macroscopic forms, on a rubbing-treated polyimide. These films have honeycomb-packed tubular pores aligned along two distinct in-plane directions with respect to the rubbing direction. In other words, these films have an in-plane zigzag mesoporous structure with a fixed kink angle. The kink angle can be tuned to some extent by finely tuning the reaction conditions. This unique mesoporous structure was unexpectedly discovered during the course of our study on macroscopic structural control of mesoporous silica films using a substrate coated with a polymer having a structural anisotropy. This structure is formed by strong interfacial interactions between the anisotropic polymeric substrate surface and surfactant molecules, and therefore, it is allowed only in a film form with macroscopic alignment of mesochannels. Although the existence of kinks has ever been reported for mesoporous silica fibers,[53,54] in which mesopores are aligned parallel to the fiber axis, the angles of the kinks have not been controlled, in contrast to our films in this report. The present results show that unique nanostructures, which can hardly be obtained through a homogeneous reaction, can be formed under heterogeneous conditions, in which the reaction takes place within a restricted environment.

These unique self-assembly processes in heterogeneous reaction systems and the consequent formation of unique structures are scientifically important because they are closely related to some important processes such as biomineralization. In addition to the scientific importance of the formation mechanism, these mesoporous silica films with such a unique porous structure may be useful in view of application. The present mesoporous silica films with a controlled zigzag structure provide highly controlled novel nanospaces. We have shown that mesoporous silica films with uniaxially aligned mesopores provide unique properties by incorporating guest species in the controlled nanospaces.[55–57] Incorporation of various guest species into these highly controlled unique zigzag-shaped nanospaces can lead to the formation of nanocomposite films with more sophisticated properties by combining the confinement effects and the structure of the nanospaces. For example, dual alignment control of fluorescent polymer chains in the zigzag mesopores may result in the formation of a new fluorescent composite film with dual polarization. Again, selective modification of incorporated guest species, which are aligned along one of the two directions of the mesopore, might be possible through a photoreaction using polarized light.

Experimental Section

Preparation of the Substrate. The polyimide that undergoes rubbing treatment contains a flexible hexamethylene group in the repeating unit, as described in our previous reports.[31–35] The

(33) Miyata, H.; Kawashima, Y.; Itoh, M.; Watanabe, M. *Chem. Mater.* **2005**, *17*, 5323.
(34) Miyata, H.; Suzuki, T.; Fukuoka, A.; Sawada, T.; Watanabe, M.; Noma, T.; Takada, K.; Mukaide, T.; Kuroda, K. *Nat. Mater.* **2004**, *3*, 651.
(35) Suzuki, T.; Miyata, H.; Watanabe, M.; Kuroda, K. *Chem. Mater.* **2006**, *18*, 4888.
(36) Yang, P.; Zhao, D.; Margolese, D.; Chmelka, B. F.; Stucky, G. D. *Nature (London)* **1998**, *396*, 152.
(37) Yang, P.; Zhao, D.; Margolese, D.; Chmelka, B. F.; Stucky, G. D. *Chem. Mater.* **1999**, *11*, 2813.
(38) Alberius, P. C. A.; Frindell, K. L.; Hayward, R. C.; Kramer, E. J.; Stucky, G. D.; Chmelka, B. F. *Chem. Mater.* **2002**, *14*, 3284.
(39) Choi, S. Y.; Mamak, M.; Coombs, N.; Chopra, N.; Ozin, G. A. *Adv. Funct. Mater.* **2004**, *14*, 335.
(40) Smarsly, B.; Grosso, D.; Brezesinski, T.; Pinna, N.; Boissière, C.; Antonietti, M.; Sanchez, C. *Chem. Mater.* **2004**, *16*, 2948.
(41) Miyata, H.; Itoh, M.; Watanabe, M.; Noma, T. *Chem. Mater.* **2003**, *15*, 1334.
(42) Urade, V. N.; Hillhouse, H. W. *J. Phys. Chem. B* **2005**, *109*, 10538.
(43) Lu, Y.; Fan, H.; Doke, N.; Loy, D. A.; Assink, R. A.; LaVan, D. A.; Brinker, C. J. *J. Am. Chem. Soc.* **2000**, *122*, 5258.
(44) Tian, B.; Liu, X.; Tu, B.; Yu, C.; Fan, J.; Wang, L.; Xie, S.; Stucky, G. D.; Zhao, D. *Nat. Mater.* **2003**, *2*, 159.
(45) Grosso, D.; Balkenende, A. R.; Albouy, P. A.; Lavergne, M.; Mazerolles, L.; Babonneau, F. *J. Mater. Chem.* **2000**, *10*, 2085.
(46) Grosso, D.; Babonneau, F.; Soler-Illia, G. J. A. A.; Albouy, P. A.; Amenitsch, H. *Chem. Commun.* **2002**, 748.
(47) Hayward, R. C.; Alberius, P. C. A.; Kramer, E. J.; Chmelka, B. F. *Langmuir* **2004**, *20*, 5998.
(48) Tolbert, S. H.; Schäffer, T. E.; Feng, J.; Hansma, P. K.; Stucky, G. D. *Chem. Mater.* **1997**, *9*, 1962.
(49) Hillhouse, H. W.; Okubo, T.; van Egmond, J. W.; Tsapatsis, M. *Chem. Mater.* **1997**, *9*, 1505.
(50) Hillhouse, H. W.; van Egmond, J. W.; Tsapatsis, M. *Langmuir* **1999**, *15*, 4544.
(51) Trau, M.; Yao, N.; Kim, E.; Xia, Y.; Whitesides, G. M.; Aksay, I. A. *Nature (London)* **1997**, *390*, 674.
(52) Melosh, N. A.; Davidson, P.; Feng, P.; Pine, D. J.; Chmelka, B. F. *J. Am. Chem. Soc.* **2001**, *123*, 1240.
(53) Wang, J.; Zhang, J.; Asoo, B. Y.; Stucky, G. D. *J. Am. Chem. Soc.* **2003**, *125*, 13966.
(54) Wang, J.; Tsung, C.-K.; Hong, W.; Wu, Y.; Tang, J.; Stucky, G. D. *Chem. Mater.* **2004**, *16*, 5169.
(55) Fukuoka, A.; Miyata, H.; Kuroda, K. *Chem. Commun.* **2003**, 284.
(56) Molenkamp, W. C.; Watanabe, M.; Miyata, H.; Tolbert, S. H. *J. Am. Chem. Soc.* **2004**, *126*, 4476.
(57) Martini, I. B.; Craig, I. M.; Molenkamp, W. C.; Miyata, H.; Tolbert, S. H.; Schwartz, B. J. *Nat. Nanotechnol.* **2007**, *2*, 647.

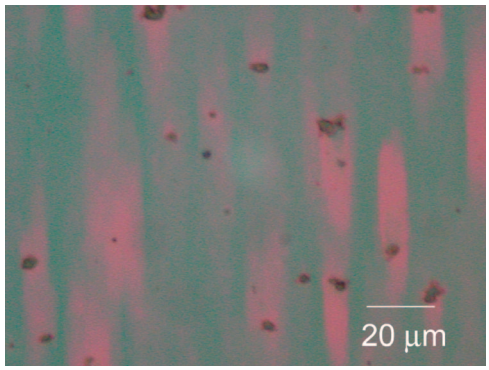

Figure 1. Optical micrograph of the mesoporous silica film.

polyimide film is formed on silica glass or silicon substrates through spin-coating of the corresponding polyamic acid and subsequent thermal imidization (200 °C, 1 h). The thickness of the polyimide was about 10 nm as determined by ellipsometry. The polyimide film on the substrate underwent rubbing treatment using a nylon-covered cylindrical roller. The details of the rubbing treatment are described elsewhere.[31]

Preparation of the Mesoporous Silica Films. The mesoporous silica films were prepared hydrothermally through heterogeneous nucleation and growth of mesostructured silica seeds on the substrate from a strongly acidic reactant solution.[32] Polyoxyethylene 10 cetyl ether ($C_{16}EO_{10}$, Brij56) was used as surfactant that works as a structure-directing agent. Tetraethoxysilane (TEOS) was mixed with a solution containing HCl, H_2O, and Brij56, and the mixture was stirred for 2.5 min at room temperature. The molar ratio is Brij56 0.0088−0.033:TEOS 0.06−0.15:HCl 3:H_2O 100. After the stirring, the mixed solution was transferred into a Teflon vessel. The vessel containing the substrate and the reactant solution was sealed at 80 °C for the growth of the mesostructured silica films. The substrate was held in the reaction solution using a substrate holder with the polyimide surface downward. The surface of the substrate was covered with another silica glass plate with a 0.2 mm gap during the film deposition. After the reaction, the film was washed with distilled water and dried in air. The surfactant was removed by calcination under an air atmosphere at 540 °C for 10 h.

Characterization. The porous structure of the films was elucidated by X-ray diffraction (XRD). Conventional $\theta-2\theta$ scanning XRD was performed with a Philips X-pert Pro using Cu Kα radiation. The in-plane XRD[58] patterns were recorded with an X-ray diffractometer equipped with a four-axes goniometer (Rigaku ATX-G) using Cu Kα radiation. The incident angle of X-rays in the in-plane geometry was set to 0.2°. The two-dimensional (2D) XRD patterns were recorded under a reflection geometry using synchrotron radiation at the Photon Factory (KEK Japan) on beamline 4A.[58] A 3 μm × 3 μm X-ray microbeam with 8 keV was used, and the diffraction patterns were recorded using an X-ray CCD detector with an image intensifier. The images of transmission electron microscopy (TEM) and scanning electron microscopy (SEM) were recorded on a Hitachi H-800 at an accelerating voltage of 200 kV and on a Hitachi S-5000H at an accelerating voltage of 5 kV, respectively.

Results

The optical micrograph of the as-grown film prepared under the conditions of $C_{16}EO_{10}/TEOS/H_2O = 0.01/0.1/100$ is shown in Figure 1. The observed texture is aligned perpendicularly to the rubbing direction. This texture is similar to that observed for the mesoporous silica films with uniaxially aligned mesoporous structures,[32] indicating the formation of an anisotropic mesoporous structure.

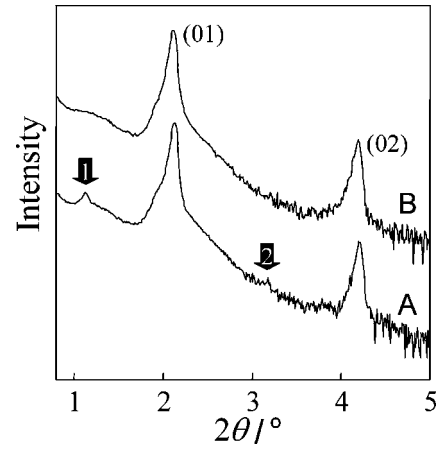

Figure 2. $\theta-2\theta$ scanning XRD profiles of the as-grown film. The projection of the incident X-rays is perpendicular (trace A) and parallel (trace B) to the rubbing direction.

Figure 2 shows the $\theta-2\theta$ scanning XRD profiles of the as-grown film prepared under the same conditions as the sample in Figure 1. The diffraction intensity is shown in log scales to display all the diffraction peaks with different intensities simultaneously. These profiles are consistent with a 2D hexagonal mesoporous structure, and the observed peaks are assigned as (01) and (02). Extra peaks are observed when the projection of the incident X-rays is perpendicular to the rubbing direction (Figure 2, trace A, indicated by arrows 1 and 2). The peak pointed by arrow 1 can be assigned as (10) and ($\bar{1}$1), and the peak pointed by arrow 2 is assigned as (11) and ($\bar{1}$2), as confirmed by the comparison with the 2D-XRD patterns shown below. These reciprocal lattice points do not contribute to the $\theta-2\theta$ scanning XRD pattern under an ideal measurement condition, but the X-ray divergence angle of ∼5°, which is comparable to the diffraction angles, makes these points observable under this geometry. Because these lattice planes are not parallel to the substrate surface, the positions of these peaks on the 2θ axis do not represent the actual distance of these lattice planes. These extra peaks ought not to be observed when the projection of the incident X-rays is perpendicular to the mesopores. Therefore, the observed difference in the $\theta-2\theta$ scanning XRD patterns, with respect to the in-plane rotation of the film, indicates the in-plane structural anisotropy of the film. A more detailed explanation of the anisotropic $\theta-2\theta$ scanning XRD patterns, caused by in-plane structural anisotropy, is shown in our previous paper.[59]

The anisotropy of the XRD profiles is much more prominent when the diffraction is measured under an in-plane geometry. Figure 3A shows the $\phi-2\theta\chi$ scanning profiles of the as-grown film. While no diffraction peaks were observed when the rubbing direction of the sample was set parallel to the projection of the incident X-rays at $\phi = 0°$, two diffraction peaks, which can be assigned as ($\bar{1}$1) and

(58) Marra, W. C.; Eisenberger, P.; Cho, A. Y. *J. Appl. Phys.* **1979**, *50*, 6927.

(59) Noma, T.; Miyata, H.; Takada, K.; Iida, A. *Adv. X-ray Anal.* **2001**, *45*, 359.

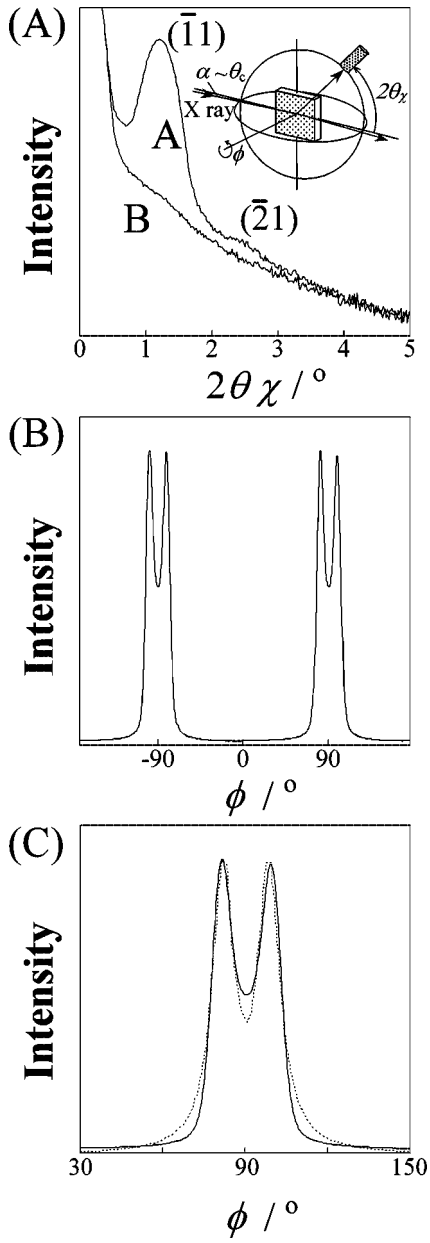

Figure 3. In-plane XRD profiles of the as-grown film. (A) $\phi-2\theta\chi$ scanning profiles. The rubbing direction was perpendicular (trace A) and parallel (trace B) to the X-rays, respectively. Inset: scanning axes of the in-plane XRD geometry. (B) ϕ scanning profile at $2\theta\chi = 1.20°$. (C) Deconvolution of the diffraction peak in the ϕ scanning profile. The solid line and the dotted line show the experimental profile and the fitted curve, respectively.

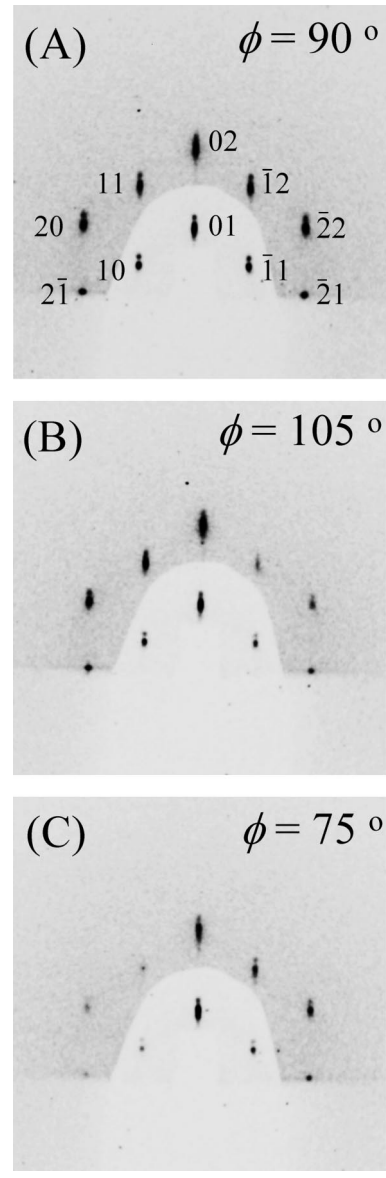

Figure 4. 2D-XRD patterns of the as-grown film recorded at different ϕ rotation angles. (A) $\phi = 90°$, (B) $\phi = 105°$, and (C) $\phi = 75°$.

$(\bar{2}1)$ by comparison with the 2D-XRD patterns shown below, were observed at $2\theta\chi = 1.20°$ and 2.40°, respectively, when the rubbing direction was perpendicular to the projection of the incident X-rays at $\phi = 0°$. The peak observed at $2\theta\chi = 1.20°$ is not caused by a lattice plane that is perpendicular to the substrate; in other words, this peak is not a real in-plane diffraction peak. Here again, the divergence of the incident X-rays, which is comparable to the diffraction angles, make this lattice plane detectable under the in-plane diffraction geometry. These observed anisotropy in the radial scanning in-plane XRD profiles is also substantially the same as that observed for the uniaxially aligned mesoporous silica film in our previous paper.[32]

However, the in-plane rocking curve recorded for this film clearly demonstrates the structural difference from the conventional uniaxially aligned mesoporous silica film, which shows two diffraction peaks with an interval of 180° in the profile. Figure 3B shows the ϕ scanning profile of the in-plane diffraction peak observed in Figure 3A. As can be seen, a pair of doublet diffraction peaks were observed at positions of $\pm(90 \pm 9°)$. Because each doublet can be deconvoluted into two Gaussian curves (Figure 3C), it is clear that the mesochannels are aligned along two distinct directions with respect to the rubbing direction. Interestingly, the intensity of the paired diffraction peaks is always the same within the error of the measurement. This obviously shows that the area of the mesoporous silica film in which the mesochannels are aligned along one direction is macroscopically the same as the area in which they are aligned along the other direction. These XRD results indicate the formation of a mesoporous silica film with regular zigzag-shaped mesochannels.

The 2D-XRD data strongly support this proposed structure. Figure 4 shows the 2D-XRD patterns of the film prepared under the conditions of $C_{16}EO_{10}$/TEOS/H_2O = 0.0088/0.1/100. The angle between the two alignment directions is

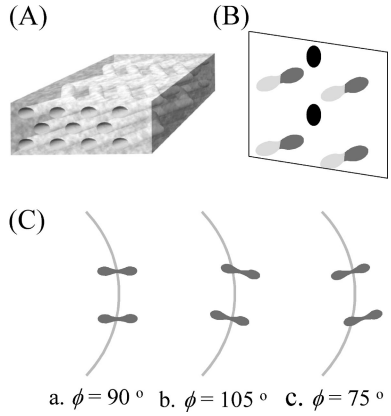

Figure 5. (A) Schematic illustration of the mesoporous silica film with a controlled zigzag porous structure. (B) Schematic illustration of the reciprocal lattice points. (C) Relationship between the reciprocal lattice points and the Ewald sphere for different rotation angle (ϕ).

estimated to be 15.5° by in-plane XRD for this film. The 2D-XRD patterns were recorded at different ϕ rotation angles. When the projection of the incident X-rays is perpendicular to the rubbing direction, at $\phi = 90°$, the diffraction spots on the left and right sides are of comparable intensity (Figure 4A), judging from the even darkness of the corresponding spots. However, when the sample is rotated along the ϕ-axis by +15°, the spots on the left side became more remarkable than those on the right side, demonstrating that the diffraction intensity of the spots on the left side becomes larger (Figure 4B). On the contrary, when the sample was rotated by −15°, the diffraction intensity of the spots in the right side becomes larger than those of the left spots (Figure 4C).

The observed change in the diffraction patterns, shown in Figure 4, is explained by the relative positions of the reciprocal lattice points with respect to the Ewald sphere. The in-plane zigzag mesoporous structure, illustrated in Figure 5A, provides the reciprocal lattice points with dumbbell-like shapes (except for the points of (01) and (02)), as schematically shown in Figure 5B. When $\phi = 0°$, the cross section of the reciprocal lattice points by the Ewald sphere is essentially the same for both sides, as schematically shown in Figure 5C(a). This explains the similar intensity of the spots on the both sides. The rotation of the sample around the ϕ-axis corresponds to the rotation of the reciprocal lattice points in the reciprocal space. When the sample is rotated in the positive direction from $\phi = 90°$, one of the spheroids of the dumbbell-shaped reciprocal lattice points on the left side intersects the surface of the Evald sphere (Figure 5C(b)). However, because of the finite curvature of the Ewald sphere, the spheroids of the dumbbell-shaped reciprocal lattice points on the right side are not on the surface of the Ewald sphere (Figure 5C(b)). In this geometry, the diffraction intensity of the left spots becomes larger than that of the right spots. When the sample is rotated in the negative direction from $\phi = 90°$, the diffraction intensity of the right spots becomes larger with the same reason (Figure 5C(c)).

The controlled zigzag porous structure of the film is retained after the surfactant removal by calcination. Although shrinkage of the periodic structure takes place along the thickness direction of the film, the in-plane structure, that is, the zigzag angle as well as the distribution of the alignment direction, is completely retained (Supporting Information, Figure S1). The direct estimation of the pore size of the film samples is quite difficult because of the too small amounts to be measured. In our previous report on a uniaxially aligned mesoporous silica film, the pore size of the film sample is represented by that of the powder sample, which is concomitantly obtained with the mesostructured silica film, and was estimated to be ∼4.2 nm on the basis of a BJH method for the sample prepared using $C_{16}EO_{10}$.[32] Because the local porous structure of the zigzag films is almost the same as that of the uniaxially aligned film, which is proven by the similar XRD pattern, we can assume that the pore size in this study is similar to that reported previously. Because the in-plane zigzag structure is independent of the existence of the surfactant, all the results and the discussion of this paper are described for uncalcined films.

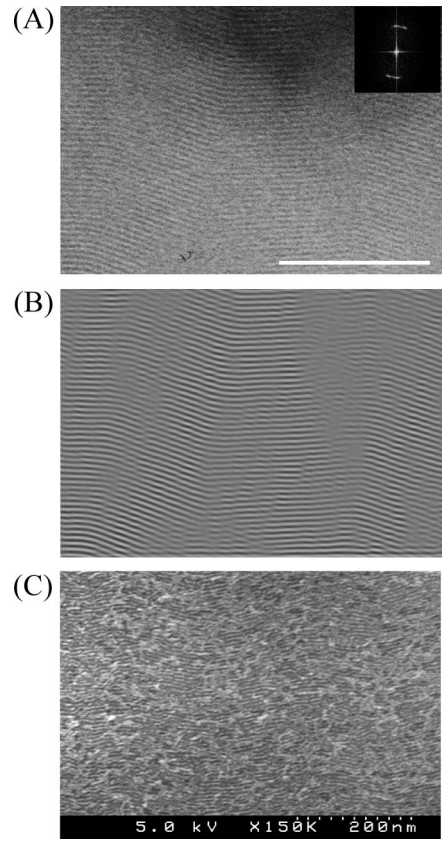

Figure 6. (A) Top view TEM image of the as-grown film. Scale bar: 100 nm. Inset: FFT image. (B) Reconstructed image of (A) from the FFT image. (C) SEM image of the surface of the as-grown film.

The porous structure of this film can be confirmed with TEM and high-resolution SEM. The plane view of TEM image of the film is shown in Figure 6A,B. Figure 6B is an image reconstructed by extracting the periodic components in the fast Fourier-transformed (FFT) image of Figure 6A. The observed zigzag porous structure is consistent with the XRD data. The FFT image shown in the inset of Figure 6A clearly shows the existence of two preferred alignment directions. The FE-SEM image, shown in Figure 6C, proves the existence of the zigzag porous structure on the top surface of the film. From the XRD results, we had expected a

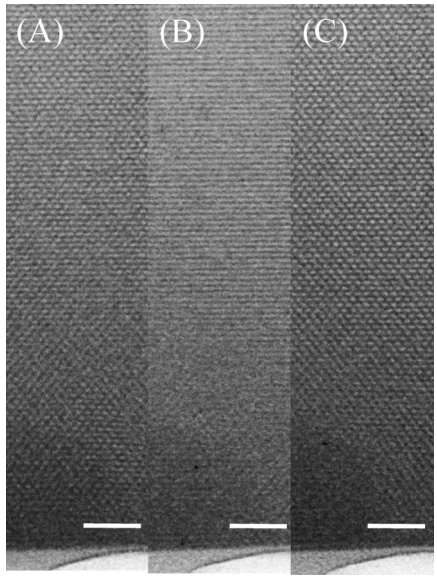

Figure 7. Cross-sectional TEM image of the as-grown film recorded with different tilt angles. The tilt angles are (A) −20°, (B) −6°, and (C) +8°. Scale bar: 50 nm.

herringbone-like zigzag structure, that is, regular linear zigzag with steep kinks, because of the identical intensity of the sharply split diffraction peaks in the in-plane ϕ scanning profile. However, it was proved, by these micrographs, that the kink is not sharp but shows some curvature. The position of the kinks is shown to be random, and only the kink angle is uniform.

The structural information along the film thickness was obtained from cross-sectional TEM study. Figure 7 shows the change of the TEM image with tilting the specimen. These images prove the formation of a honeycomb-packed porous structure over the whole thickness of the film of ∼500 nm. The honeycomb structure is observable with two tilt angles (Figure 7A,C), and stripelike images are observed between the two angles (Figure 7B). This undoubtedly shows that the tubular pores are aligned along two independent directions. These images were obtained because the interval of the zigzag structure, which is ∼100 nm, is smaller than the specimen thickness, which is 200–300 nm; that is, these are superimposed images of the several areas in which the mesopores are aligned along the two different directions.

Through comprehensive modification of the preparation conditions, it was shown that the molar ratio of TEOS in the reactant solution is a critical parameter for the kink angle of the in-plane zigzag structure. The in-plane kink angle (distance of the split peaks in the ϕ scanning profiles, $\Delta\phi$) is plotted against the molar ratio of TEOS, as shown in Figure 8. It is demonstrated that the in-plane kink angle increases with the increase of the molar ratio of TEOS in the reactant solution. The increase of the kink angle with the TEOS molar ratio is observed for the reactant solutions with the surfactant concentrations of Brij56/H_2O = 0.01/100 and 0.03/100. For the samples prepared from the lower surfactant concentration (Brij56/H_2O = 0.01/100), the split of the ϕ scanning profile is observed when the TEOS/H_2O ratio is in the range 0.06–0.15. On the other hand, the split is observed when the TEOS/H_2O ratio is between 0.1 and 0.15 for the samples

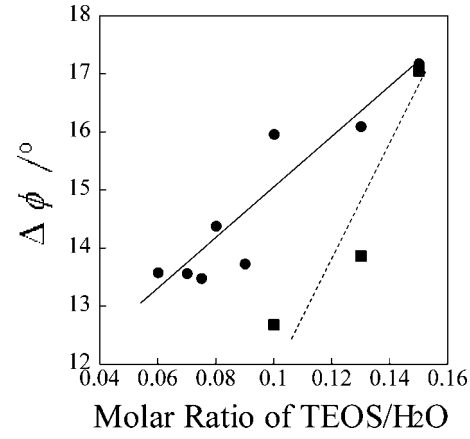

Figure 8. Dependence of the molar ratio of TEOS/H_2O on the folding angle of the in-plane zigzag structure. Circles, solid line: Brij56/H_2O = 0.01/100; rectangles, broken line: Brij56/H_2O = 0.03/100.

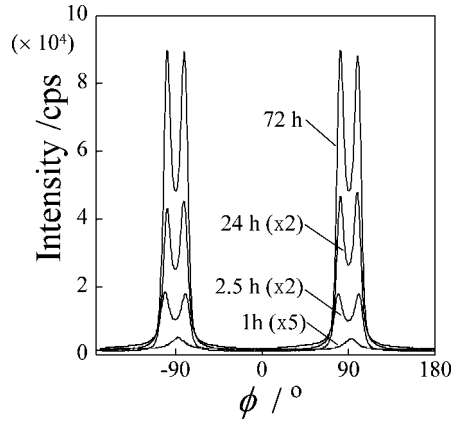

Figure 9. ϕ scanning profiles of the films in the early stages of the film formation.

prepared from higher surfactant concentration (Brij56/H_2O = 0.03/100). The dependence of the $\Delta\phi$ on the surfactant concentration indicates that the surfactant molar ratio is also an important parameter for the formation of the zigzag porous structure.

In order to investigate the formation mechanism of the controlled zigzag mesoporous structure, the early stages of the film formation were investigated. Figure 9 shows the change of the in-plane ϕ scanning profile. Although the peak is broad, no split was observed in the profile of the film after 1 h film growth, showing that the initial structure is not the zigzag structure but the mesopores are aligned perpendicularly to the rubbing direction. However, the profile of the film after 2.5 h growth is apparently split, demonstrating that the zigzag structure is formed at relatively early stages of the film formation.

Discussion

Equivalent Four Diffraction Peaks in the ϕ Scanning In-Plane XRD Profile. The same intensity of the four diffraction peaks in the in-plane ϕ scanning XRD profiles, shown in Figures 3B and 9, shows that each area with one of the two alignment directions of the mesochannels is the same. However, the positions of the kinks are not regular, as proved by the TEM and the FE-SEM images in Figure 6. These two facts seem to be inconsistent with each other

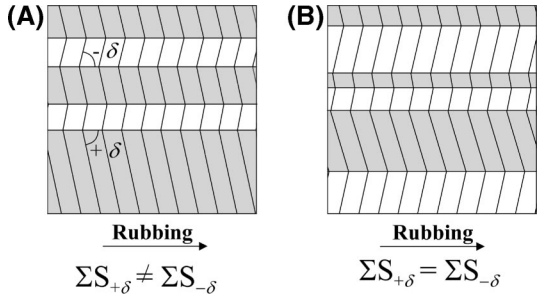

Figure 10. Models of the porous structures when the diffraction intensity of the split peaks is different (A) and identical (B).

because the areas with the respective alignment directions are likely to depend on the positions of the kinks. When the positions of the kinks are random, the area in which the mesochannels are aligned with an angle of $+\delta$ with respect to the normal direction of the rubbing treatment would not be necessarily the same as the area in which the mesochannels are aligned with an angle of $-\delta$, although the bending angle is constant (Figure 10A). However, when the linear mesochannels, which are aligned perpendicularly to the rubbing direction, were bent with a constant angle, fixing both edges on the substrate, the areas with the above two alignment directions become always the same independent of the positions of the kinks (Figure 10B). In fact, the mesochannels are aligned perpendicularly to the rubbing direction at the initial stages of the film formation. Therefore, it is shown that the transformation from the uniaxially aligned mesoporous structure into the zigzag structure can explain the observed equivalent intensity of the four diffraction peaks in the in-plane ϕ scanning profiles.

Formation Mechanism of the Zigzag Porous Structure with Fixed Kink Angles. At a very early stage of the film formation, a uniaxially aligned mesoporous structure was formed, as shown in Figure 9. For the formation of such mesoporous silica films with a uniaxially aligned porous structure, we have proposed a model that the surfactant molecules are adsorbed parallel to the rubbing direction through hydrophobic interactions with the elongated and aligned polymer chains on the substrate.[31] The tubular mesopores are formed perpendicularly to the rubbing direction because the long axis of a tubular micelle is perpendicular to the alkyl chains of each surfactant molecule. At early stages of the film formation, the structure is flexible, and the hydrolyzed silica source would easily diffuse into the structure because of the immature condensation of silica.

The bending of the tubes takes place for the uniaxially aligned initial structure with immaturely condensed silica walls. The surfactant molecules would be anchored parallel to the direction of the polymer chains through strong hydrophobic interactions. The energy regarding the adsorption is minimum when the alkyl chain of the surfactant is parallel to the polymer chains on the surface, and it increases with the deviation angle from the direction of the polymer chains. However, the increase of the energy would be much smaller for translational movement that does not accompany the change of the adsorption direction. It is considered that the rotational movement of the adsorbed molecules with respect to the direction of the polymer chains is unlikely,

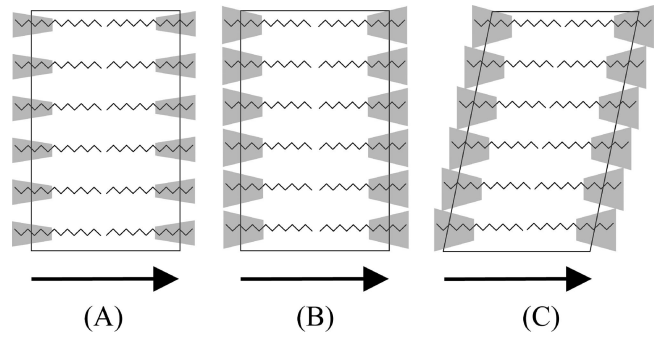

Figure 11. Schematic illustration of the formation mechanism of the controlled zigzag porous structure. Zigzag line depicts the surfactant molecule, and the gray trapezoids depict the silica oligomers. Straight tubular structure in the early stages of the film formation (A, B) transfers into the zigzag structure through the parallel shift of the surfactant molecules to the rubbing direction by increase of the size of the hydrophilic part (C).

and the surfactant molecules would keep the adsorption state parallel to the rubbing direction even after the bending of the mesochannels. This means that, at least in the first layer, the surfactant molecules are not perpendicular to the direction of the mesochannels. Although a twist from the parallel adsorption state is unlikely, a parallel shift of the molecular position along the rubbing direction would take place much easier. It is considered that the surfactant molecules on the substrate surface move along the rubbing direction when the mesochannels are bent. However, from the second layer on, surfactant molecules might be perpendicular to the long axes of the mesochannels, that is, not parallel to the rubbing direction, because their direction would not be directly restricted by the anisotropic polymer surface. From the experimental results shown above, we propose the formation mechanism of the zigzag mesoporous structure as shown in Figure 11.

When the substrate with a rubbing-treated polyimide film is soaked in the reactant solution, the surfactant molecules are adsorbed on the polymeric substrate surface through hydrophobic interactions. It should be noted that the surfactant molecules adsorbed on the substrate are a minority because most of the surfactant molecules assemble in the reactant solution to form a surfactant−silica composite through homogeneous nucleation and growth. The hydrolyzed silica oligomers in the solution interact with the hydrophilic head groups of the surfactant adsorbed on the substrate as well as those in the solution. At the early stages of the film formation, the size of the silica oligomers that interact with the hydrophilic head groups of the surfactant is relatively small because of their relatively high charge density. The uniaxially aligned mesostructure is geometrically allowed at this stage (Figure 11A). The progress of the condensation of silanol groups in the silica oligomers decreases their charge density, and charged soluble siliceous species are supplied from the solution to keep the charge balance. Consequently, the size of the silica oligomers that interact with one surfactant headgroup increases (Figure 11B). Under the conditions employed in this study, the size of the hydrophilic part would exceed the limit that allows the retention of the initial straight tubular micelle structure. However, the distance between the adjacent surfactant molecules cannot increase because the surfactant molecules

are anchored on the substrate surface and the displacement traversing the polymer chains is highly unlikely. Then, the surfactant molecules would shift along the polyimide molecular chains, which are aligned by the rubbing treatment, to avoid steric overlapping (Figure 11C). Although the attractive interactions between the surfactant molecules and the polymeric surface are quite strong, the surfactant molecules would be able to slide along the direction of the polymer chains, as described above.

This model is consistent with the observed dependence of the kink angle on the TEOS concentration. That is, the size of the silica oligomers that interact with the head groups of one surfactant molecule increases with the increase of TEOS concentration, and consequently, the enhanced steric effect increases the kink angle of the zigzag structure.

The observed dependence of the kink angle on the surfactant concentration is also consistent with the proposed model. The silica oligomers in the solution are consumed by the formation of the surfactant−silica composite both in the solution and on the substrate, and the distribution is determined by the ratio of the surfactant existing in the solution and those adsorbed on the substrate. For a given amount of TEOS, more silica oligomers are consumed for the formation of the surfactant−silica composite particles, through homogeneous nucleation and growth, in a reactant solution for higher surfactant concentration. This is because of the fact that only a small fraction of the dissolved surfactant is adsorbed on the substrate surface. Consequently, the size of the silica oligomers that interact with the head groups decreases with the increase of the surfactant concentration. This is the reason why the kink angle of the zigzag porous structure prepared under the higher surfactant conditions is smaller, as shown in Figure 8. When the concentration of silica oligomer becomes high enough, the dependence on the surfactant concentration becomes negligible, and consequently, the kink angle of the zigzag structure becomes independent of the surfactant concentration.

The observed zigzag porous structure is formed under the conditions in which the surfactant concentration is very low compared to that for the formation of a mesoporous silica film with uniaxially aligned tubular pores. When the concentration of the surfactant is high, the interactions between the surfactant molecules adsorbed on the surface are strong because of the higher adsorption density. The increased attractive interactions of the adsorbed surfactant molecules would prevent the displacement of the molecules along the polymer chains and the consequent formation of the zigzag porous structure.

Recently, the formation of mesoporous silica with helical porous structures was reported using a nonchiral surfactant by simply decreasing the surfactant concentration.[60] We consider that the present zigzag structure is closely related to such mesoporous silicas with helical mesochannels.

Conclusion

Mesoporous silica films with a controlled zigzag porous structure are prepared. The tubular mesopores are bent with a fixed angle over the whole of the film. This is confirmed by the existence of four well-resolved diffraction peaks in the in-plane ϕ scanning profiles. The zigzag porous structure is formed under considerably dilute surfactant concentrations, and the kink angle is shown to be dependent on the TEOS/surfactant molar ratio in the reactant solution. This zigzag mesoporous structure is formed via the immature uniaxially aligned 2D hexagonal structure, at the initial stages of the film formation, and it is shown that the progress of the condensation of silica under the spatially confined conditions causes the observed zigzag porous structure. The mesoporous silica films with such unique porous structure are useful for unique alignment control of various guest species, and for the related applications, through anisotropic accommodation in the controlled nanospaces.

Acknowledgment. The authors acknowledge Mr. Y. Ishida and Dr. Y. Murata (Canon Inc.) for the SEM observation and drawing computer graphics. The authors also acknowledge Prof. O. Terasaki (Stockholm University) and Prof. T. Ohsuna (Waseda University) for useful discussions. The authors thank Dr. O. Albrecht (Canon Inc.) for careful reviewing of the manuscript. The work was partially supported by the 21st Century COE Program "Practical Nano-Chemistry" from MEXT, Japan. This work was done in part at the "Center for Practical Chemical Wisdom" supported by the Global COE program of MEXT. This work is also supported by A3 Foresight Program "Synthesis and Structural Resolution of Novel Mesoporous Materials" from Japan Society for the Promotion of Science (JSPS). T.S. is grateful for financial support via a Grant-in-Aid for JSPS from MEXT.

Supporting Information Available: Figure of XRD profiles of the calcined mesoporous silica film. This information is available free of charge via the Internet at http://pubs.acs.org.

CM702120M

(60) Wang, B.; Chi, C.; Shan, W.; Zhang, Y.; Ren, N.; Tang, Y. *Angew. Chem., Int. Ed.* **2006**, *45*, 2088.